GEOPHYSICAL RESEARCH LETTERS, VOL. 35, L09202, doi:10.1029/2008GL033388, 2008

Observation of atmospheric tides in the Martian exosphere using Mars Reconnaissance Orbiter radio tracking data

E. Mazarico,[1] M. T. Zuber,[1,2] F. G. Lemoine,[2] and D. E. Smith[2]

Received 28 January 2008; revised 13 March 2008; accepted 24 March 2008; published 7 May 2008.

[1] Based on the perturbations of the trajectory of the Mars Reconnaissance Orbiter due to atmospheric drag, we estimate, using Precision Orbit Determination, the density of the Martian exosphere near 250 km altitude with much better temporal (and therefore spatial) resolution than previously possible with this method. Small longitudinal density variations are observed to be consistent over long time periods. Although they appear fixed with respect to the planet, we interpret them as non-migrating tides because of the Sun-synchronous spacecraft orbit. Similar tides were observed previously by MGS at much lower altitude (~125 km), and our results agree to first order with the MGS findings. **Citation:** Mazarico, E., M. T. Zuber, F. G. Lemoine, and D. E. Smith (2008), Observation of atmospheric tides in the Martian exosphere using Mars Reconnaissance Orbiter radio tracking data, *Geophys. Res. Lett.*, *35*, L09202, doi:10.1029/2008GL033388.

1. Introduction

[2] The density of the Martian exosphere (i.e. the neutral atmosphere above ~200 km) cannot be sampled by conventional remote sensing or in situ methods (thermal spectrometers, accelerometers). Recent studies using Precision Orbit Determination on high altitude orbiting spacecraft provided valuable insight on that region of the atmosphere where escape occurs [*Konopliv et al.*, 2006; *Forbes et al.*, 2006; *Mazarico et al.*, 2007]. However, these studies were severely limited in temporal resolution; due to the very low density levels at the orbital altitude and the resulting small drag perturbations on the spacecraft trajectory, measurements could be obtained daily at best. With its much lower orbital altitude (~250 km compared to ~400 km for Mars Global Surveyor, MGS, and Mars Odyssey, ODY), the Mars Reconnaissance Orbiter (MRO) [*Zurek and Smrekar*, 2007] offers an opportunity to obtain similar measurements but at much higher temporal, and therefore spatial, resolution.

2. Data and Methods

[3] We use the trajectory analysis program GEODYN II [*Pavlis et al.*, 2006] to perform the study. We processed the dataset in short periods (called 'arcs'). Each arc is forward-integrated using a number of highly accurate a priori physical models. The spacecraft initial state and various model parameters are then iteratively modified until the modeled trajectory best fits the observational constraints provided by the radio tracking data. The 1s-averaged X-band Doppler data from MRO provide dense coverage, thanks in part to the quality of the 1-way data enabled by the onboard Ultra-Stable Oscillator (USO) [*Zuber et al.*, 2007a]. The range data are very sparse (~6,000 measurements over ~1 year, compared to ~17 million Doppler observations). Among the adjusted parameters, the drag coefficient C_D is used to scale the atmospheric density predicted by the a priori atmospheric model [*Stewart*, 1987]. Because the orbit of MRO is lower than those of MGS and ODY, the gravity field models obtained previously [*Lemoine*, 2003; *Konopliv et al.*, 2006] are not appropriate for small force recovery. Short-wavelength gravity anomalies not significant at 400 km altitude become important at 250 km. We used a recent solution obtained from ~6 years of MGS data and one year of MRO data [*Zuber et al.*, 2007b]. We also improved the modeling of the non-conservative forces (atmospheric drag, solar, albedo and planetary thermal radiation pressures) by including the effects of inter-plate self-shadowing in the cross-section calculations. It is particularly important for MRO because of its large 3-m-diameter High-Gain Antenna (HGA): the cross-sectional area entering the model equations for the solar radiation and the atmospheric drag accelerations can be overestimated by ~20% and ~30% respectively when not considering the effects of self-shadowing [*Mazarico*, 2008]. The errors are entirely propagated into the adjusted small force scale factors and can therefore contribute significant errors to the measured density. Highly variable self-shadowing, as in the case of the atmospheric drag for MRO, can also affect the orbital perturbation signature of non-conservative forces, and modify the way GEODYN distributes their individual contributions.

3. Data Processing

[4] No or few radio observations were available in the few weeks surrounding the October 2006 conjunction, so the analysis period began on November 3rd, 2006 (DOY_{2006} = 307). We processed approximately one year of radio tracking data from the primary science phase, until October 19th, 2007. The viewing geometry from the Earth was increasingly favorable for drag recovery, best when the orbit is viewed edge-on.

[5] The force mismodelings are commonly due to the small, non-conservative accelerations. The actual atmospheric density experiences high-frequency, and sometimes large, changes compared to the predictions (the model by *Stewart* [1987] is a very simple semi-analytical model based on Mariner 9 and Viking data). Short arc durations are

[1]Department of Earth, Atmospheric and Planetary Sciences, Massachusetts Institute of Technology, Cambridge, Massachusetts, USA.
[2]Solar System Exploration Division, NASA Goddard Space Flight Center, Greenbelt, Maryland, USA.

0094-8276/08/2008GL033388$05.00

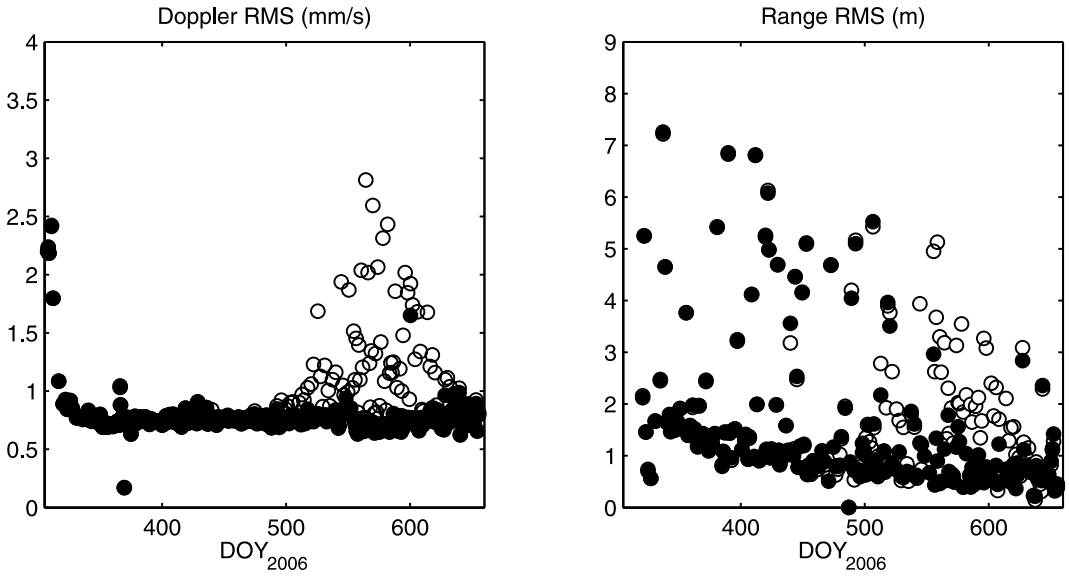

Figure 1. Root-Mean Square (RMS) of the tracking data observations: (left) Doppler in mm/s and (right) range in m. The open circles show the RMS of the initially recovered arcs. Upon exit of the solar conjunction ($DOY_{2006} \sim 300$), the RMS values rapidly decrease. The large increase for $DOY_{2006} > 500$, due to density enhancement related to the dust storm season, is removed completely after adjusting for cyclic along-track accelerations (filled circles).

preferable in order to minimize the perturbations induced on the reconstructed orbit. Our arcs are generally shorter than 1 day, which is compatible with the frequent density estimates.

[6] The scale factor for the solar radiation pressure (C_R) is well-determined and close to 1, indicating good force modeling. The relatively large densities enable the adjustment of the predicted densities at frequencies up to once every two orbits (i.e. ~4 hours). The situation is much more favorable than in the case of Mars Odyssey, for which the atmospheric drag was two orders of magnitude smaller than the solar radiation pressure [*Mazarico et al.*, 2007]. For MRO, the magnitudes of the two forces are similar, but when considering only the along-track component the atmospheric drag dominates by one order of magnitude. The uncertainties of the recovered density values are 0.1 to 1% at 4-h temporal resolution (and smaller at lower estimation frequencies). Shorter estimation periods (one orbit, i.e. ~2 h) lead to poor density recovery, high relative uncertainties and sometimes unreasonable values.

[7] The Root-Mean Square (RMS) values of the observation residuals of the converged arcs are generally small: ~0.7–0.8 mm/s for the Doppler; ~2 m for the Range (Figure 1). However, we observe a significant increase in RMS (to about 3 mm/s) in the second half of the time series. The increase coincides with a density enhancement in the southern hemisphere due to the Summer 2007 dust storm, and can be attributed to short-comings of the a priori atmospheric model (which does not include dust storms). To compensate, we added empirical periodic (1-cycle per orbit) along-track accelerations in the orbit determination process. For each arc, an amplitude and a phase are estimated. The RMS values are reduced to nominal, and the phasing of the acceleration (maximum near periapsis, located near the south pole) is consistent with the expected dust storm effect on density. Thus, we added the equivalent density contribution of those empirical accelerations to our total measurements.

4. Atmospheric Results

4.1. Recovered Densities

[8] The 4-hour density measurements that we obtained (Figure 2) are remarkably consistent given that each arc is analyzed independently. In addition to the expected seasonal trend (model predictions in Figure 2), the effect of the Summer 2007 dust storm is clearly visible. The solar activity over the entire period is very low (solar minimum), which may explain why we do not observe the solar rotation periodicity noted previously by *Forbes et al.* [2006] and *Mazarico et al.* [2007] from MGS and ODY data respectively (moreover, the altitude sampled was much higher in both cases). The scatter around the seasonal trend is related to the atmospheric variability. For the 4-h time series, the estimated relative variability ranges between 5 and 15% (maximum near the beginning and near the end of the analyzed time period; minimum near $DOY_{2006} \sim 520$; see Figure 3c).

4.2. Atmospheric Sampling

[9] Due to the slight orbit eccentricity and the periapsis location (~87°S), most of the drag on the spacecraft is encountered in the southern hemisphere. The drag is maximum near the south pole, but is still half of that near 20°S, so the southern low to mid-latitudes regions contribute as well. The south polar region is sampled every orbit because of the 92.8° inclination of MRO's orbit. Therefore, the densities shown in Figure 2 are referenced at a point 250 km above the south pole. This fixed location prevents orbital changes in periapsis altitude, etc. from affecting the time series and its interpretation. In addition, given the strong dependence of the exospheric temperature on the

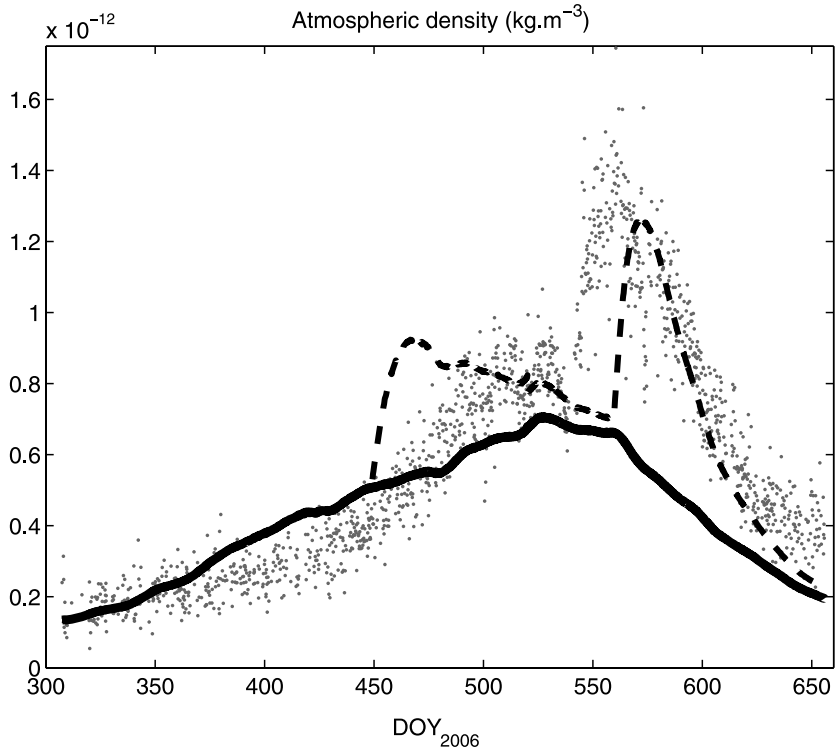

Figure 2. Recovered total density measurements (4-h temporal resolution) compared to the *Stewart* [1987] model (solid line) and modified Stewart with Viking-like dust storms (dashed line).

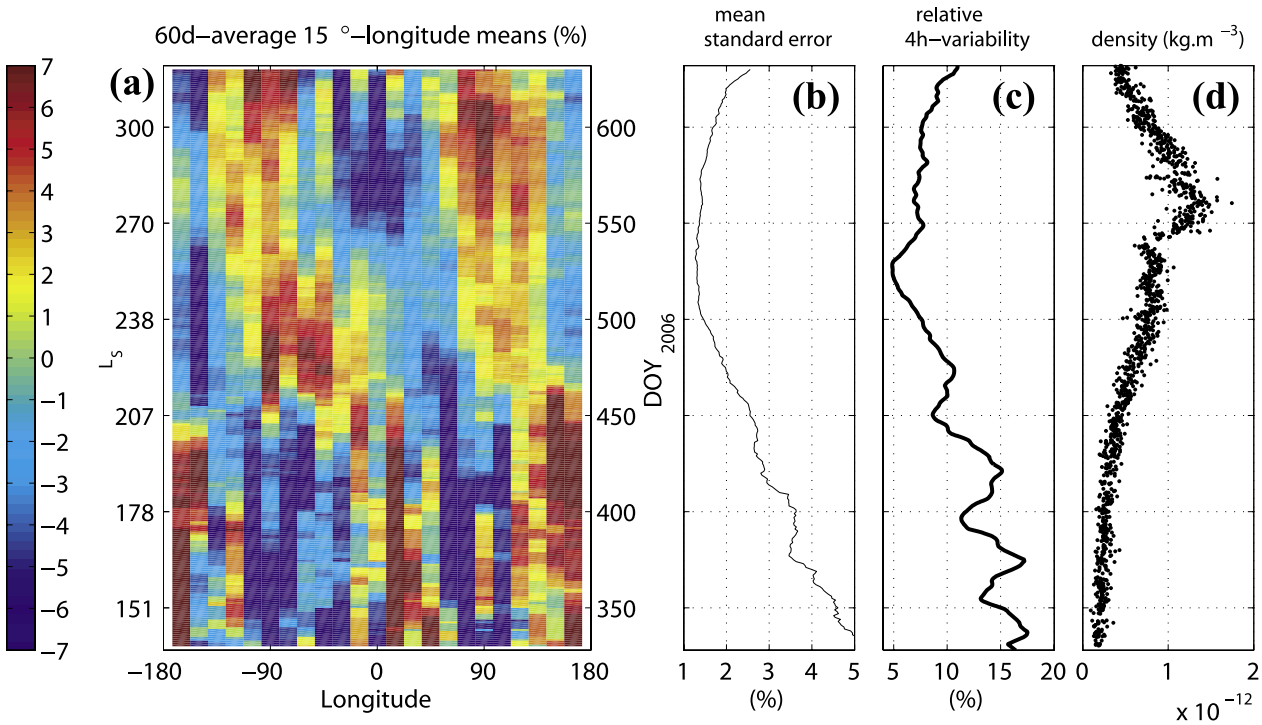

Figure 3. (a) Mean of density residuals over 60 days and 15° longitude. We successively translated the 60-day window by 1-day increments to obtain this figure. The color bar shows the residual magnitude in percent (compared to the density level in the same 60-day window). The ability to recover the wave structure is hindered by the background atmospheric variability: (b) standard mean error of the residual means in Figure 3a and (c) relative atmospheric variability (in %), which was obtained by smoothing the 30-day running standard deviation of the density time series. For convenience, (d) the absolute density from Figure 2 is also shown.

local solar time, the day side contributes significantly more of the total atmospheric drag than the night side. To first order, it is thus possible to assume the measurements to principally reflect the density of specific longitudes. We assign each 4-h density measurement the equator-crossing dayside longitude (not very different from the periapsis longitude given the low-altitude polar orbit).

4.3. Longitudinal Variations

[10] We obtain density residuals by removing the long-period density trend from the measurements. Due to the high level of background variability, 60 days of measurements were combined to obtain robust estimates of the longitudinal variations. We present the mean density residuals in 15° longitude bins (Figure 3a) and the associated average 'mean standard errors' (Figure 3b). The early period, with low density and high variability, is not very favorable to the recovery of a small signal, but the signal-to-noise ratio improves during the southern summer dust storm season (see Figures 3c and 3d). A coherent pattern in longitude, with a ~6% amplitude, is visible in Figure 3, especially for $DOY_{2006} > 450$ when the density is high and the relative variability is low. This latter period coincides with the conditions described by *Bougher et al.* [1993] (solar minimum, southern summer dust season) most favorable to the observation of tides near the exobase. In addition to the clear wavenumber 2 pattern, wavenumber 1 was found to greatly reduce the RMS of the fit, while higher orders do not contribute. The fits for the amplitudes and phases have small uncertainties: respectively for waves 1 and 2, $\sim 0.92 \pm 0.65\%$ and $\sim 0.75 \pm 0.42\%$ for the amplitudes, and $\sim 22 \pm 14°$ and $\sim 10 \pm 7°$ for the phases.

5. Preliminary Interpretation

[11] Both amplitude and phase are well-constrained and consistent over periods much longer than 60 days, which gives us confidence in the observation of the atmospheric tides. There are several short-lived periods of low-amplitude values, but they are probably artifacts of the 60-day fitting. Nevertheless, the phase shift (Figure 3a) between the southern spring ($L_S = 180°$ to $L_S = 270°$) and summer ($L_S = 270°$ to $L_S = 360°$) appears to be real, and could be related to seasonal changes in the zonal wind structure of the lower atmosphere.

[12] The tides themselves appear to be fixed with respect to the planet, as the longitudinal patterns are consistent over ~60 days in the body-fixed frame. However, the orbit of MRO is Sun-synchronous, such that the spacecraft ground track is always observed at the same local solar time (3 am/pm for MRO), so they are most likely non-migrating tides. Such tides arise from the interaction of the solar radiation with zonal body-fixed heterogeneities. They were previously observed on Mars during the aerobraking phase of MGS, near 125 km altitude [*Keating et al.*, 1998; *Forbes and Hagan*, 2000; *Wilson*, 2002; *Withers et al.*, 2003]. Atmospheric tides were generally not thought to propagate into the exosphere, even though transport and molecular conduction are recognized to be more important processes in the Martian atmosphere than in Earth's [*Bougher and Roble*, 1991].

[13] Nevertheless, the effects of damping are significant. We do not observe any contribution of wavenumber 3, which dominated the total density variations at lower altitude [*Withers et al.*, 2003]. This is consistent from what can be expected from the Hough mode study of *Withers et al.* [2003] (cf. their Figure 17): the appropriate modes responsible for wave 3 non-migrating tides have shorter vertical wavelengths, so they are strongly damped. On the other hand, some of the Hough modes that potentially force waves 1 and 2 have long vertical wavelength, so we expect smaller damping and potential observation near 250 km. The amplitudes of the waves observed by the MGS accelerometer experiment are also compatible to first order with our results. We estimate wave amplitudes near 250 km altitude from data between 130 and 160km of *Withers et al.* [2003, Figure 6]. Whether we consider the total density variations or only wavenumber 2, we obtain a range of predicted wave amplitude between 2 and 8% of the total density. This is in close agreement with our results (~6%), and strengthens our confidence in the wave structure observed with MRO.

6. Conclusion and Future Work

[14] The radio tracking dataset of the Mars Reconnaissance Orbiter has enabled the accurate recovery of numerous atmospheric density measurements over the mission's primary science phase (November 2006 to October 2007). The low orbital altitude and relatively high atmospheric drag environment allow frequent estimation of density which results in unprecedented longitudinal resolution. Under favorable conditions (solar minimum, dust storm season, local solar time of 3 pm), non-migrating atmospheric waves are observed to propagate up into the exosphere. With the increasing solar activity of the new solar cycle, current atmospheric models predict that those waves will diminish in importance, and may disappear, due to the stronger *in situ* solar forcing in the exosphere. The timing of their disappearance may provide information on the mechanism(s) that control the structure of the exosphere.

[15] In the future, we will use numerical results of the MTGCM [*Bougher et al.*, 2000] to further interpret the measurements obtained with MRO. This General Circulation Model has been successful in generating wave activity in the aerobraking region [*Bougher et al.*, 1999, 2006]. In addition to determining if waves similar to those found from the tracking data near 250 km (amplitude, phasing) are predicted numerically, it can be helpful in better understanding how our sampling (tied to the spacecraft orbit) affects the recovery of these waves.

[16] **Acknowledgments.** This work was supported by the NASA Mars Critical Data Products program and the NASA Mars Reconnaissance Orbiter Project.

References

Bougher, S. W., and R. G. Roble (1991), Comparative terrestrial planet thermospheres: 1. Solar cycle variation of global mean temperatures, *J. Geophys. Res.*, *96*(A7), 11,045–11,055.

Bougher, S. W., C. G. Fesen, E. C. Ridley, and R. W. Zurek (1993), Mars mesosphere and thermosphere coupling: Semidiurnal tides, *J. Geophys. Res.*, *98*(E2), 3281–3295.

Bougher, S., G. Keating, R. Zurek, J. Murphy, R. Haberle, J. Hollingsworth, and R. T. Clancy (1999), Mars Global Surveyor aerobraking: Atmospheric trends and model interpretation, *Adv. Space Res.*, *23*, 1887–1897.

Bougher, S. W., S. Engel, R. G. Roble, and B. Foster (2000), Comparative terrestrial planet thermospheres: 3. Solar cycle variation of global structure and winds at solstices, *J. Geophys. Res.*, *105*(E7), 17,669–17,692.

Bougher, S. W., J. M. Bell, J. R. Murphy, M. A. Lopez-Valverde, and P. G. Withers (2006), Polar warming in the Mars thermosphere: Seasonal variations owing to changing insolation and dust distributions, *Geophys. Res. Lett.*, *33*, L02203, doi:10.1029/2005GL024059.

Forbes, J. M., and M. E. Hagan (2000), Diurnal Kelvin wave in the atmosphere of Mars: Towards an understanding of 'stationary' density structures observed by the MGS accelerometer, *Geophys. Res. Lett.*, *27*(21), 3563–3566.

Forbes, J. M., S. Bruinsma, and F. G. Lemoine (2006), Solar rotation effects in the thermospheres of Mars and Earth, *Science*, *312*, 1366–1368, doi:10.1126/science.1126389.

Keating, G. M., et al. (1998), The structure of the upper atmosphere of Mars: In situ accelerometer measurements from Mars Global Surveyor, *Science*, *279*, 1672–1676.

Konopliv, A. S., C. F. Yoder, E. M. Standish, D.-N. Yuan, and W. L. Sjogren (2006), A global solution for the Mars static and seasonal gravity, Mars orientation, Phobos and Deimos masses, and Mars ephemeris, *Icarus*, *182*, 23–50, doi:10.1016/j.icarus.2005.12.025.

Lemoine, F. G. (2003), 'mgm1041c' gravity field solution, http://pds-geosciences.wustl.edu/geodata/mgs-m-rss-5-sdp-v1/mors_1021/sha/, *Geosci. Node, Planet, Data Syst.*, Washington Univ., St. Louis, Mo.

Mazarico, E. (2008), Study of the Martian upper atmosphere using radio tracking data, Ph.D. thesis, 236 pp. Mass. Inst. of Technol., Cambridge.

Mazarico, E., M. T. Zuber, F. G. Lemoine, and D. E. Smith (2007), Martian exospheric density using Mars Odyssey radio tracking data, *J. Geophys. Res.*, *112*, E05014, doi:10.1029/2006JE002734.

Pavlis, D. E., S. G. Poulose, and J. J. McCarthy (2006), GEODYN operations manuals, contractor report, Stinger Ghaffarian Technol., Greenbelt, Md.

Stewart, A. I. F. (1987), Revised time dependent model of the Martian atmosphere for use in orbit lifetime and sustenance studies, *Tech. Rep. JPL PO NQ-802429*, Univ. of Colo., Boulder.

Wilson, R. J. (2002), Evidence for nonmigrating thermal tides in the Mars upper atmosphere from the Mars Global Surveyor Accelerometer Experiment, *Geophys. Res. Lett.*, *29*(7), 1120, doi:10.1029/2001GL013975.

Withers, P., S. W. Bougher, and G. M. Keating (2003), The effects of topographically-controlled thermal tides in the Martian upper atmosphere as seen by the MGS accelerometer, *Icarus*, *164*, 14–32, doi:10.1016/S0019-1035(03)00135-0.

Zuber, M. T., F. G. Lemoine, D. E. Smith, A. S. Konopliv, S. E. Smrekar, and S. W. Asmar (2007a), Mars Reconnaissance Orbiter radio science gravity investigation, *J. Geophys. Res.*, *112*, E05S07, doi:10.1029/2006JE002833.

Zuber, M. T., R. J. Phillips, J. C. Andrews-Hanna, S. W. Asmar, A. S. Konopliv, F. G. Lemoine, J. J. Plaut, D. E. Smith, and S. E. Smrekar (2007b), Density of Mars' south polar layered deposits, *Science*, *317*, 1718–1719, doi:10.1126/science.1146995.

Zurek, R. W., and S. E. Smrekar (2007), An overview of the Mars Reconnaissance Orbiter (MRO) science mission, *J. Geophys. Res.*, *112*, E05S01, doi:10.1029/2006JE002701.

F. G. Lemoine and D. E. Smith, Solar System Exploration Division, NASA Goddard Space Flight Center, Greenbelt, MD 20771, USA.

E. Mazarico and M. T. Zuber, Department of Earth, Atmospheric and Planetary Sciences, Massachusetts Institute of Technology, 77 Massachusetts Avenue, Cambridge, MA 02139, USA. (mazarico@alum.mit.edu)